JACS
JOURNAL OF THE AMERICAN CHEMICAL SOCIETY

Subscriber access provided by American Chemical Society

Article

Fluorescence Quenching of Dyes by Tryptophan: Interactions at Atomic Detail from Combination of Experiment and Computer Simulation

Andrea C. Vaiana, Hannes Neuweiler, Andreas Schulz, Jrgen Wolfrum, Markus Sauer, and Jeremy C. Smith

J. Am. Chem. Soc., **2003**, 125 (47), 14564-14572• DOI: 10.1021/ja036082j • Publication Date (Web): 04 November 2003

Downloaded from http://pubs.acs.org on March 30, 2009

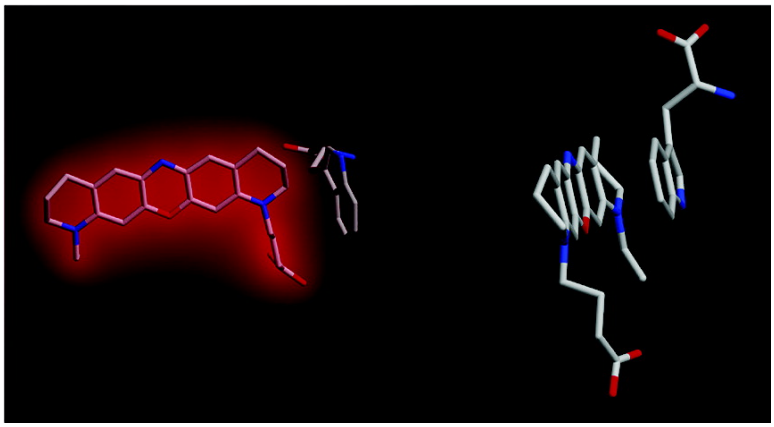

More About This Article

Additional resources and features associated with this article are available within the HTML version:

- Supporting Information
- Links to the 8 articles that cite this article, as of the time of this article download
- Access to high resolution figures
- Links to articles and content related to this article
- Copyright permission to reproduce figures and/or text from this article

View the Full Text HTML

ACS Publications
High quality. High impact.

Journal of the American Chemical Society is published by the American Chemical Society. 1155 Sixteenth Street N.W., Washington, DC 20036

J|A|C|S
ARTICLES
Published on Web 11/04/2003

Fluorescence Quenching of Dyes by Tryptophan: Interactions at Atomic Detail from Combination of Experiment and Computer Simulation

Andrea C. Vaiana,[†] Hannes Neuweiler,[§] Andreas Schulz,[§] Jürgen Wolfrum,[§] Markus Sauer,[§] and Jeremy C. Smith*,[†]

Contribution from the IWR-Computational Molecular Biophysics, Universität Heidelberg, Im Neuenheimer Feld 368, D-69120 Heidelberg, Germany, and Physikalisch-Chemisches Institut, Universität Heidelberg, Im Neuenheimer Feld 253, D-69120 Heidelberg, Germany

Received May 12, 2003; E-mail: biocomputing@iwr.uni-heidelberg.de

Abstract: Fluorescence spectroscopy and molecular dynamics (MD) simulation are combined to characterize the interaction of two organic fluorescent dyes, rhodamine 6G (R6G) and an oxazine derivative (MR121), with the amino acid tryptophan in aqueous solution. Steady-state and time-resolved fluorescence quenching experiments reveal the formation of essentially nonfluorescent ground-state dye/Trp complexes. The MD simulations are used to elucidate the molecular interaction geometries involved. The MD-derived probability distribution of the distance r between the centers of geometry of the dye and quencher ring systems, $P(r)$, extends to higher distances for R6G than for MR121 due to population in the R6G/Trp system of fluorescent interaction geometries between Trp and the phenyl ring and ester group of the dye. The consequence of this is the experimental finding that under the conditions used in the simulations about 25% of the R6G dye is fluorescent in comparison with 10% of the MR121. Combining the above findings allows determination of the "quenching distance", r^*, above which no quenching occurs. r^* is found to be very similar (~5.5 Å) for both dye/Trp systems, corresponding to close to van der Waals contact. Both experimental dynamic Stern−Volmer analysis and the MD trajectories demonstrate that the main determinant of the fluorescence intensity is static quenching. The approach presented is likely to be useful in the structural interpretation of data obtained from fluorescent conjugates commonly used for monitoring the binding and dynamics of biomolecular systems.

1. Introduction

The development of innovative fluorescence-based techniques for probing molecular recognition and conformational dynamics of biopolymers is of major interest in biophysical chemistry. The naturally occurring amino acid tryptophan (Trp) is of particular interest in fluorescence-based work on peptides and proteins. For example, the quenching of the triplet state of Trp by cysteine has been used to measure the rate of formation of specific intramolecular contacts in disordered peptides.[1] Moreover, Trp can serve as an efficient electron donor in photoinduced electron transfer (PET) reactions with certain dye molecules, a property conferred by the Trp indole side chain which is the most readily oxidized functional group among all naturally occurring amino acids.[2] In an example of the use of PET, it has been shown that efficient PET between Trp and riboflavin in the binding pocket of the riboflavin-binding protein can be used to detect different conformational states of the protein.[3] In the crystal structure of this complex, Trp and riboflavin are oriented in a stacked face-to-face geometry enabling ultrafast charge transfer between their aromatic moieties.

In further promising applications, PET-based biosensors have been developed that use conformationally induced alterations in PET efficiency upon binding for the specific detection of DNA or RNA sequences or antibodies at the single-molecule level.[4,5] These biosensors take advantage of specific properties of naturally occurring DNA nucleotides and amino acids, in particular, the low oxidation potential of Trp and the DNA base guanosine and the tendency of many fluorophores to aggregate in aqueous environment to decrease their water-accessible surface area. In contrast to electronic energy transfer-based systems, in which long-range dipole−dipole interactions occur, the above sensors require contact formation between the fluorophore and the guanosine or tryptophan residue. Depending on the reduction potential of the fluorophore used, efficient fluorescence quenching via PET can then occur. With careful design of conformationally flexible molecules and the use of

[†] IWR-Computational Molecular Biophysics.
[§] Physikalisch-Chemisches Institut.

(1) Lapidus, L. J.; Steinbach, P. J.; Eaton, W. A.; Szabo, A.; Hofrichter, J. *J. Phys. Chem. B* **2002**, *106*, 11628−11640.
(2) Jones, G.; Lu, L. N.; Vullev, V.; Gosztola, D. J.; Greenfield, S. R.; Wasielewski, M. R. *Bioorg. Med. Chem. Lett.* **1995**, *5*, 2385−2390.
(3) Zhong, D.; Zewail, A. H. *Proc. Natl. Acad. Sci. U.S.A.* **2001**, *98*, 11867−11872.
(4) Neuweiler, H.; Schulz, A.; Vaiana, A. C.; Smith, J. C.; Kaul, S.; Wolfrum, J.; Sauer, M. *Angew. Chem., Int. Ed.* **2002**, *41*, 4769−4773.
(5) Knemeyer, J. P.; Marme, N.; Sauer, M. *Anal. Chem.* **2000**, *72*, 3717−3724.

10.1021/ja036082j CCC: $25.00 **© 2003 American Chemical Society**

appropriate fluorophores (rhodamine and oxazine dyes are well-suited), efficient single-molecule sensitive PET sensors can be produced. For example, if quenching interactions between the fluorophore and the guanosine or tryptophan residue are hindered upon specific binding to the target (for example, due to binding of a complementary DNA sequence or antibody or due to cleavage by an endonuclease or protease enzyme) the fluorescence of the sensor is restored. In addition to detecting the presence of a target, the contact-induced quenching process can also be used to monitor the rate of intramolecular contact formation in peptides or the opening/closing dynamics of DNA hairpins at the single-molecule level.[6] Therefore, PET-based molecules are ideally suited for single-molecule studies and offer an elegant alternative to conventional biosensors based on electronic energy transfer processes.

Contact formation between Trp and the dye is signaled by a strong quenching of dye fluorescence. To correlate fluorescence spectroscopic data recorded from dye-labeled Trp-containing peptides or proteins with conformational properties, a detailed understanding of the relation between fluorescence quenching by Trp and the underlying interaction geometries is necessary. A complete theoretical understanding of PET reactions and fluorescence quenching in fluorophore/quencher complexes would in principle require accurate quantum chemical calculations of ground and excited-state properties of the complexes involved, including the effects of the surrounding environment. Although the speed and accuracy of quantum chemical methods is ever increasing, these calculations are still computationally too expensive to permit incorporation of complex environmental effects, and they are presently mostly limited to the treatment of relatively small, isolated molecules. One recent example of this is the use of time-dependent density functional theory to describe the fluorescence quenching and lifetimes involved in stacking interactions of 2-aminopurine with purines and pyrimidines.[7] Molecular dynamics (MD) simulations have the advantage over quantum chemical methods of computational speed. Thus, although MD is unable to model the electronic transitions involved in excited-state kinetics, it does allow the incorporation of environmental effects such as explicit solvent molecules together with extensive configurational averaging. Since pioneering work in which fluorescence anisotropy decays of the six Trp residues of lysozyme were examined by MD simulation,[8] a number of MD studies of fluorophores in complex environments have been reported, including a MD study relating the fluorescence quenching and the dynamical behavior of a flavin adenine dinucleotide molecule,[9] several studies of the quenching of tryptophan fluorescence in proteins and peptides,[10−14] and a mixed quantum chemical/molecular mechanics study of the variability of the fluorescence quantum yield of

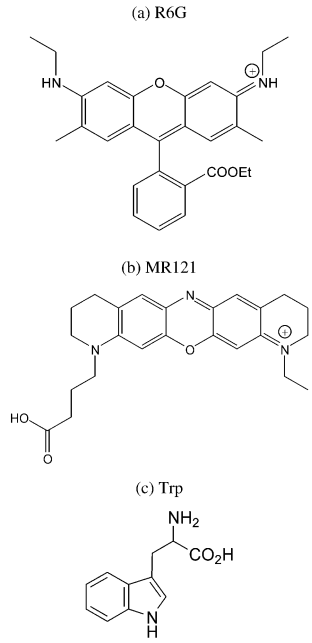

Figure 1. Chemical structures of the two dyes and of the amino acid Trp: (a) R6G, (b) MR121, and (c) Trp.

Trp in proteins.[15] Studies concerning the simulations of organic dye structures and their interactions with biomolecules are rare; this is most probably due to the difficulty of developing new force field parameters for dye molecules. Only a few of these studies exist, such as the simulation of the solvation behavior of coumarin 153[16] and of the dynamics of fluorescein in an antibody binding site.[17]

Here we report a combined experimental fluorescence spectroscopy and MD study of the bimolecular interaction of two organic dyes, Rhodamine 6G (Figure 1a) and the oxazine derivative MR121 (Figure 1b), with Trp (Figure 1c) in aqueous solution. Steady-state and time-resolved fluorescence intensities were measured as a function of Trp concentration, allowing extraction of thermodynamic and kinetic quenching parameters via Stern−Volmer analysis. These parameters are interpreted using MD simulation of the two systems in conditions designed to match the experiments as closely as possible. To enable the simulations to be carried out, it was necessary to derive force-field parameters for the dyes. This was performed using the Automated Frequency Matching Method.[18] The MD simulations, in explicit solvent, enabled two-dimensional potentials of mean force, $\omega(r,\varphi)$ (where r is the distance between the centers of geometry of the dye and quencher ring systems and φ the angle between the normals to the ring planes), to be determined with good statistical accuracy. Significant differences are found both in the experimental effective binding constants and in the simulation-derived potentials of mean force. Interestingly, combining these two quantities, both of which yield information on the probability distributions of different states of the dye/quencher system, leads to the same ring separation cutoff distance, ∼5.5 Å, for fluorescence quenching. A physical explanation of the interactions involved is made possible via

(6) Neuweiler, H.; Schulz, A.; Böhmer, M.; Enderlein, J.; Sauer, M. *J. Am. Chem. Soc.* **2003**, *125*, 5324−5330.
(7) Jean, J. M.; Hall, K. B. *Proc. Natl. Acad. Sci. U.S.A.* **2001**, *98*, 37−41.
(8) Ichiye, T.; Karplus, M. *Biochemistry* **1983**, *22*, 2884−2893.
(9) van den Berg, P. A. W.; Feenstra, K. A.; Mark, A. E.; Berendsen, H. J. C.; Visser, A. J. W. G. *J. Phys. Chem. B* **2002**, *106*, 8858−8869.
(10) Bismuto, E.; Martelli, P. L.; Casadio, R.; Irace, G. *Protein Sci.* **2000**, *9*, 1730−1742.
(11) Laboulais, C.; Deprez, E.; Leh, H.; Mouscadet, J.-F.; Brochon, J.-C.; Le Bret, M. *Biophys. J.* **2001**, *81*, 473−489.
(12) Yeh, I.-C.; Hummer, G. *J. Am. Chem. Soc.* **2002**, *124*, 6563−6568.
(13) Muino, P. L.; Harris, D.; Berryhill, J.; Hudson, B.; Callis, P. R. *Proc. SPIE-Int. Soc. Opt. Eng.* **1992**, *1640*, 240−251.
(14) Ludescher, R. D.; Peting, L.; Hudson, S.; Hudson, B. *Biophys. Chem.* **1987**, *28*, 59−75.
(15) Callis, P. R.; Vivian, J. T. *Chem. Phys. Lett.* **2003**, *369*, 409−414.
(16) Cichos, F.; Brown, R.; Rempel, U.; von Borczyskowski, C. *J. Phys. Chem. A* **1999**, *103*, 2506−2512.
(17) Lim, K.; Herron, J. N. *Biochemistry* **1995**, *34*, 6962−6974.
(18) Vaiana, A. C.; Schulz, A.; Wolfrum, J.; Sauer, M.; Smith, J. C. *J. Comput. Chem.* **2003**, *24*, 632−639.

the $\omega(r,\varphi)$ plots. Finally, the experimental kinetic parameters are compared with quenching kinetics determined from MD time series analysis: both indicate nanosecond time scale lifetimes of the fluorescent states. The combination of simulation and experiment presented here allows the derivation of a detailed geometric and dynamic model of fluorescence quenching of the dyes by Trp, an approach that will be widely applicable in the interpretation of spectroscopic data recorded from dye-labeled Trp-containing biopolymers, in studies aimed at determining biomolecular structure and dynamics from fluorescence measurements.

2. Methods

2.1. Experimental Procedure. Fluorescence measurements of R6G and MR121 in the presence of different Trp concentrations were performed using standard fluorescence spectrometers. All measurements were performed at room temperature (25 °C) in aqueous solution of phosphate-buffered saline (PBS, pH 7.4). Steady-state fluorescence intensities were recorded with a fluorescence spectrometer LS100 from Photon Technology Int. (Wedel, Germany). Corrected fluorescence spectra were obtained using a high-pressure xenon flash lamp as the excitation source. Ensemble fluorescence lifetimes, τ, were measured with a standard spectrometer from IBH (model 5000MC; Glasgow, U.K.) for time-correlated single-photon counting (TCSPC) using a pulsed diode laser (635 nm) as the excitation source (4096 channels, 12.5 ps/channel, 5000 photons in the maximum channel). To exclude polarization effects, fluorescence was observed under the magic angle (54.7°). The decay parameters were determined by least-squares deconvolution, and their quality was judged by the reduced χ^2 values and the randomness of the weighted residuals. In the present systems the decays were well fitted by a monoexponential function:

$$I(t) = I(0)\exp(-t/\tau) \quad (1)$$

where τ is the lifetime of the excited species and $I(t)$ is the measured fluorescence intensity at time t after excitation. Because of the time resolution limit of the apparatus, strongly quenched populations with decay times shorter than ~50 ps were not detectable.

2.2. Simulations. 2.2.1. Force Field. All molecular mechanics and dynamics computations were performed using CHARMM version 27.[19] The CHARMM potential energy function is given by:

$$V(R) = \sum_{\text{bonds}} K_b(b-b_0)^2 + \sum_{\text{ub}} K_{ub}(s-s_0)^2 + \sum_{\text{angles}} K_\theta(\theta-\theta_0)^2 + \sum_{\text{dihedrals}} K_\chi(1+\cos(n\chi-\chi_0)) + \sum_{\text{impropers}} K_\varphi(\varphi-\varphi_0)^2 + \sum_{\text{nonbond}} \left\{ \epsilon_{ij}\left[\left(\frac{R_{ij}^{\min}}{r_{ij}}\right)^{12} - \left(\frac{R_{ij}^{\min}}{r_{ij}}\right)^{6}\right] + \frac{q_i q_j}{r_{ij}} \right\} \quad (2)$$

where K_b, K_{ub}, K_θ, K_χ, K_φ are the bond, Urey−Bradley, angle, dihedral, and improper dihedral force constants, respectively, and b, s, θ, χ, and φ represent the bond lengths, Urey−Bradley 1−3 distances, bond angles, dihedral angles, and improper torsion angles, respectively. The subscript zero, where present, is used to represent the corresponding equilibrium value. Nonbonded interactions between pairs of atoms (labeled i and j) at a relative distance r_{ij} are described by the Lennard-Jones 6−12 and Coulombic interaction terms; $R_{ij}^{\min}$ is the distance between atoms i and j at which the Lennard-Jones potential is zero, and ϵ_{ij} is related to the depth of the Lennard-Jones potential well for the same pair of atoms. q_i is the partial atomic charge on atom i.

Parameters for R6G and MR121 were derived using the Automated Frequency Matching Method (AFMM) described in ref 18. The AFMM method involves refinement of an initial parameter set by fitting to match vibrational eigenvectors and eigenvalues derived from quantum-chemical normal mode calculations. AFMM has already been successfully used to derive CHARMM force field parameters for polycyclic molecules.[18,20] The force field parameter derivation for R6G is described in ref 18. Here we apply the method to derive force-field parameters for MR121, a recently synthesized oxazine dye.[21] No force field parameter set has yet been developed for this molecule. Furthermore, suitable experimental data on which to base a parametrization for MR121 do not exist. Hence, the parametrization scheme used here relies solely on reference data from high-level quantum chemical calculations. All quantum chemical calculations required for parametrization of MR121 were performed with the GAUSSIAN-94 package using the standard 6-31G* basis set[22] and the restricted Hartree−Fock (RHF) level of theory for both geometry optimizations and normal mode calculations.

An initial set of parameters for MR121 was selected for refinement using AFMM. The partial atomic charges, q_i in eq 2, were derived using the CHELPG methodology[23] with a standard RHF/6-31G* quantum chemical optimization. The CHELPG method employs a least-squares fitting procedure to determine the set of atomic partial charges that best reproduces the quantum mechanical electrostatic potential at selected grid points around the molecule. Three new atom types were defined to describe the nitrogens and the oxygen present on the ring system of the dye (see Figure 1b). The van der Waals constants ϵ_{ij} and $R_{ij}^{\min}$ for these were directly transferred from original CHARMM values for NC2, NN3G, and OS atom types (see refs 24−26). van der Waals constants and partial atomic charges were not modified during refinement. Equilibrium values for bonds b_0, angles θ_0, and dihedrals χ_0 that were not present in the original CHARMM force field parameter set[24−26] were derived from the structure resulting from the RHF/6-31G* optimization. An initial guess, based on analogy to similar existing CHARMM parameters and on chemical intuition, was made for all other missing parameters. All force field parameters not given in refs 24−26 are available as Supporting Information.

The initial parameter set was used for minimization and calculation of normal modes (eigenvalues and eigenvectors) with CHARMM.[27] In the force field parameter derivation calculation, all molecular mechanics minimizations were carried out using the Steepest Descent algorithm followed by Newton−Raphson minimization with a convergence criterion for the energy gradient of 10^{-8} kcal/mol/Å. The normal modes obtained were compared with the normal modes calculated with the quantum chemical method, which are considered to be the reference. Parameters were then refined iteratively to fit the results of the quantum chemical normal mode eigenvalues and vectors.

(19) Brooks, B.; Bruccoleri, R.; Olafson, B.; States, D.; Swaminathan, S.; Karplus, M. *J. Comput. Chem.* **1983**, 187−217.
(20) Cournia, Z.; Vaiana, A. C.; Smith, J. C.; Ullmann, M. *Pure Appl. Chem.* **2003**.
(21) Sauer, M.; Zander, C.; Muller, R.; Gobel, F.; Schulz, A.; Siebert, S.; Drexhage, K. H.; Wolfrum, J. *Proc. SPIE-Int. Soc. Opt. Eng.* **1997**, *2985*, 61−68.
(22) Frisch, M. J.; Trucks, G. W.; Schlegel, H. B.; Gill, P. M. W.; Johnson, B. G.; Robb, M. A.; Cheeseman, J. R.; Keith, T.; Petersson, G. A.; Montgomery, J. A.; Raghavachari, K.; Al-Laham, M. A.; Zakrzewski, V. G.; Ortiz, J. V.; Foresman, J. B.; Cioslowski, J.; Stefanov, B. B.; Nanayakkara, A.; Challacombe, M.; Peng, C. Y.; Ayala, P. Y.; Chen, W.; Wong, M. W.; Andres, J. L.; Replogle, E. S.; Gomperts, R.; Martin, R. L.; Fox, D. J.; Binkley, J. S.; Defrees, D. J.; Baker, J.; Stewart, J. P.; Head-Gordon, M.; Gonzalez, C.; Pople, J. A. *Gaussian 94*, revision D.4; Gaussian, Inc.: Pittsburgh, PA, 1995.
(23) Breneman, C. N.; Wiberg, K. B. *J. Comput. Chem.* **1990**, *11*, 361−373.
(24) Foloppe, N.; MacKerell, A. D., Jr. *J. Comput. Chem.* **2000**, *21*, 86−104.
(25) MacKerell, A. D., Jr.; Banavali, N. *J. Comput. Chem.* **2000**, *21*, 105−120.
(26) MacKerell, A. D., Jr.; Bashford, D.; Bellott, M.; Dunbrack, R. L., Jr.; Evanseck, J. D.; Field, M. J.; Fischer, S.; Gao, J.; Guo, H.; Ha, S.; Joseph-McCarthy, D.; Kuchnir, L.; Kuczera, K.; Lau, F. T. K.; Mattos, C.; Michnick, S.; Ngo, T.; Nguyen, D. T.; Prodhom, B.; Reiher, I. W. E.; Roux, B.; Schlenkrich, M.; Smith, J. C.; Stote, R.; Straub, J.; Watanabe, M.; Wiorkiewicz-Kuczera, J.; Yin, D.; Karplus, M. *J. Phys. Chem. B* **1998**, *102*, 3586−3516.
(27) Brooks, B. R.; Janezic, D.; Karplus, M. *J. Comput. Chem.* **1995**, *16*, 1522−1542.

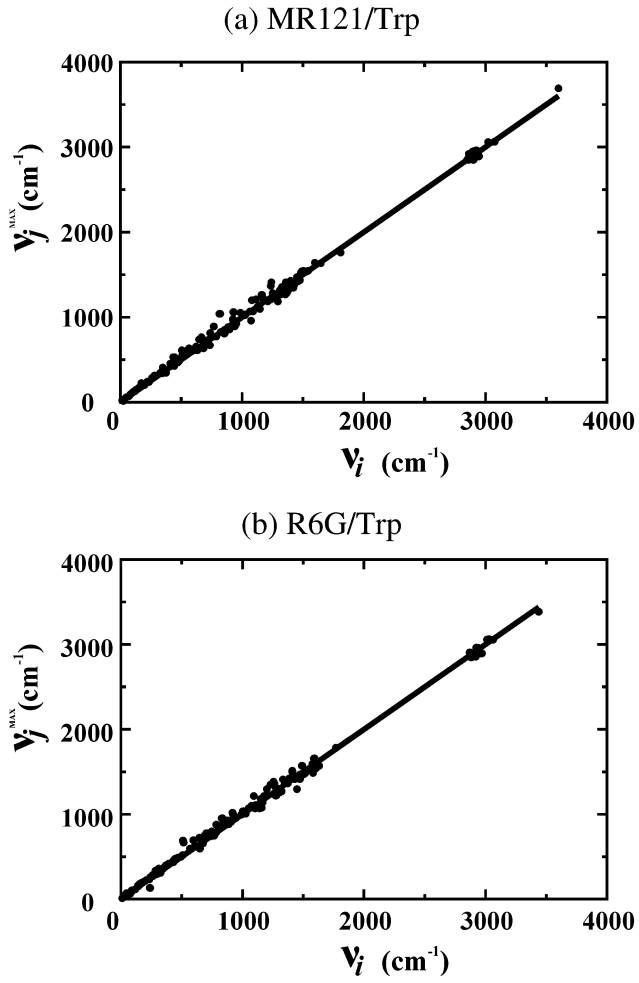

Figure 2. ν_i^{max} vs ν_i plot for MR121 (a) and R6G (b). Lines refer to the ideal case of perfectly matched frequencies and eigenvector projections; points refer to the parameters used in this work.

The AFMM method optimizes frequency matching by using a penalty function that takes into account both frequencies and all the corresponding eigenvectors. We denote the eigenvectors calculated from the MM force field as $\overline{\chi_C^i}$ and the eigenvectors calculated from the quantum chemical method as $\overline{\chi_Q^j}$, where the superscripts i and j represent the normal mode number. An efficient way to check simultaneously for both orthonormality and frequency matching is to project each of the CHARMM eigenvectors, $\overline{\chi_C^i}$, onto the reference set of eigenvectors, $\overline{\chi_Q^j}$, and to find the frequency, ν_j^{max}, corresponding to the highest projection (j: $\overline{\chi_C^i}\cdot\overline{\chi_Q^j}$ = max). In the ideal case of a perfect fit, $\nu_i = \nu_j^{max}$ and $\overline{\chi_C^i}\cdot\overline{\chi_Q^j} = \delta_{ij}$, where δ_{ij} is the Kronecker delta. The ν_i vs ν_j^{max} plot obtained with the parameter set for MR121 used here is shown in Figure 2a, along with the same plot for R6G (Figure 2b, data taken from ref 18). Values of the root-mean-square deviation from the reference case are 54.8 cm^{-1} for MR121 and 51.1 cm^{-1} for R6G. These values are within the range seen in previous benchmark studies on small aromatic compounds.[18]

The AFMM method optimizes intramolecular vibrations to reproduce the ground-state properties of a molecule in a vacuum. To model intermolecular interactions AFMM uses, as do most other MM parametrization methods, the correct reproduction by the partial atomic charges of the electrostatic potential as calculated quantum mechanically, together with the Lennard-Jones parameters. The Lennard-Jones parameters used here were transferred from existing CHARMM parameters that were derived from experimental solvation free energies and quantum chemical calculations on small model compounds.[25] The combination of AFMM, CHELPG for the atomic charges, and standard CHARMM Lennard-Jones parameters has proven to successfully reproduce sensitive intermolecular properties such as the crystal structures of both R6G[18] and cholesterol (Z. Cournia, personal communication).

2.2.2. Molecular Dynamics Simulations. MD simulations were performed on two model dye/Trp systems: the first (MR121/Trp) consisting of one MR121 dye molecule, one Trp molecule, 1013 TIP3P[28] water molecules, and a chloride counterion and the second (R6G/Trp) consisting of one R6G molecule, one Trp molecule, 1002 TIP3P[28] water molecules, and a chloride counterion.

In a recent MD study of intrapeptide interactions it was noted that the TIP3P model underestimates the viscosity of water, and the calculated time constants were thus scaled.[12] However, whereas the dynamics involved in ref 12 occurs over a long time scale and has large amplitude, that studied here is faster and more local, resulting from close-range, atomic-level interactions between the dyes and the Trp molecule that mostly involve small numbers of water molecules. Thus, viscosity plays no clear role in determining the relaxation times examined here, and no results were scaled.

Five MD simulations were performed on each of the two dye/tryptophan systems. In what follows, the simulations are referred to as RT1, ..., RT5 for the R6G/Trp system and MT1, ..., MT5 for the MR121/Trp system. For each system, the five simulations were performed with different initial ring separations so as to improve configurational statistics, as described below. All simulations were performed in the NPT ensemble at 1.0 atm pressure and at 300 K in a truncated octahedral box of (33.6 ± 0.1) Å for MR121/Trp and (33.9 ± 0.1) Å for R6G/Trp using periodic boundary conditions. This corresponds to relative Trp concentrations of 55 mM for the MR121/Trp system and 57 mM for R6G/Trp. Long-range electrostatic interactions were computed using the Particle Mesh Ewald (PME) method.[29]

The heating and equilibration procedure was the same for all the MD runs. An arbitrary starting configuration of solvated dye/tryptophan including counterions was gradually heated from 0 to 300 K during 5.5 ps, reassigning velocities every 100 steps using an integration time step of 0.1 fs. The integration time was then increased to 1 fs, and a first 100-ps equilibration was performed at constant volume and temperature. The system was then allowed to relax to its equilibrium density at constant temperature and pressure for 100 ps. At this point the distance r, between the geometrical centers of the main ring systems of the dye and of the tryptophan (the definition of r is shown in Figure 3a), was subjected to a harmonic constraint $C(r) = k(r - r_0)^2$ with the force constant k set to 10 kcal/mol/Å^2 for a total of 100 ps. Values of the equilibrium distance r_0 were 3.5 Å for RT1 and MT1, 5.0 Å for RT2 and MT2, 7.5 Å for RT3 and MT3, 10.0 Å for RT4 and MT4, and 12.5 Å for RT5 and MT5. Subsequently, the system was allowed to relax unconstrained for another 100 ps prior to the production phase.

During the production runs no constraints were used. Each production run lasted 10 ns, i.e., 50 ns of simulation time was run in total on each dye/Trp system. Altogether, the simulations required 41 days (wall time) on 32 CPUs (16 per dye/Trp system) of the HELICS cluster of the Interdisziplinäres Zentrum für Wissenschaftliches Rechnen at the University of Heidelberg. Configurations were downloaded to disk every 0.1 ps for subsequent analysis.

2.2.3. Potential of Mean Force: Theoretical Background. The mutual arrangement of the two molecules (Trp and dye) is here described by the distance r defined above and the angle φ between the normals to the planes of the main ring systems of the dye and the tryptophan (see Figure 3a). The MD simulations were used to determine the two-dimensional potential of mean force (PMF) landscape, $\omega(r,\varphi)$. This allows the free-energy differences between the complexed and

(28) Jorgensen, W.; Chandrasekhar, J.; Madura, J.; Impey, R.; Klein, M. *J. Chem. Phys.* **1983**, *79*, 926−935.
(29) Essmann, U.; Perera, L.; Berkowitz, M. L.; Darden, T.; Lee, H.; Pedersen, L. G. *J. Chem. Phys.* **1995**, *103*, 8577−8593.

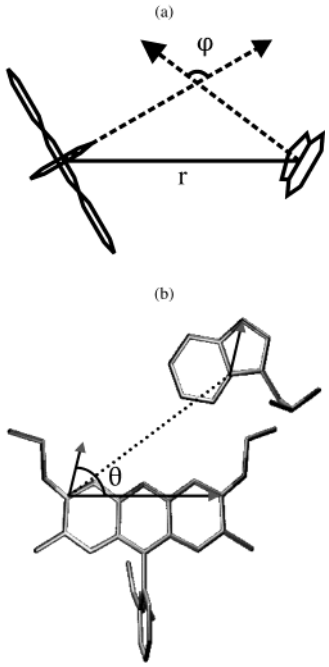

Figure 3. (a) Definitions of the dye/Trp distance, r, and the angle, φ, between the normals to the dye and Trp planes. (b) Definition of the angle, θ, between two fixed vectors lying on the dye and Trp planes. The R6G/Trp system is depicted here. The same definitions are used for the MR121/Trp system.

noncomplexed states of the dye/Trp system and the configurational pathways and free energy barriers connecting these states to be determined.

The simulation models a classical thermodynamic system in the NPT ensemble: its microscopic states are described by a set of $3N$ coordinates $\{r, \varphi, q_1, ..., q_{3N-2}\}$ and their associated momenta $\{p_r, p_\varphi, p_1, ..., p_{3N-2}\}$. At equilibrium, the probability $P(r, \varphi)$ of finding the system in a given state of the $\{r, \varphi\}$ subspace, i.e., the probability of finding given values of r and φ is:

$$P(r,\varphi) = \frac{\int_V \cdots \int \exp[-U(r,\varphi,q^1,...,q^{3N-2})/kT]\, dq_1 ... dq_{3N-2}}{Z} \quad (3)$$

where k is the Boltzmann constant, T is the temperature of the system, $U(r, \varphi, q_1, ..., q_{3N-2})$ is the potential energy, and Z is the reduced partition function. The integrals are extended to the hypervolume V of phase space spanned by all degrees of freedom except r and φ. $\omega(r,\varphi)$, the associated PMF,[30] is given by:

$$\omega(r,\varphi) = -kT \ln[P(r,\varphi)] \quad (4)$$

The negative gradient of $\omega(r,\varphi)$ with respect to r and/or φ, $-\nabla_{r,\varphi}\, \omega(r,\varphi)$, is the mean "thermodynamic drive" acting on the system along the coordinates r, φ, or both averaged over all possible states of the remaining $3N - 2$ degrees of freedom. Thus, $\omega(r,\varphi)$ is a free energy i.e., the reversible work done on the system in moving it from state (r_a,φ_a) to state (r_b,φ_b) is expressed by the difference $\Delta\omega^{a,b} = \omega(r_b,\varphi_b) - \omega(r_a,\varphi_a)$.

$P(r,\varphi)$ can be estimated using MD simulation. If $n(r,\varphi)$ is the number of MD snapshots in which the system is found to be in a volume element $d\Omega = 2\pi r^2 \sin\varphi\, dr\, d\varphi$ around position (r,φ), then $P(r,\varphi)$ is given by:

$$P(r,\varphi) \approx \frac{n(r,\varphi)}{N_{MD}\, d\Omega} \quad (5)$$

where N_{MD} is the total number of MD snapshots taken during the simulation. If the system is ergodic, the equality in eq 5 is exact in the limit $N_{MD} \rightarrow \infty$.

In the present work, for both systems simulated $n(r,\varphi)$ was evaluated on a 100 × 100 square grid over 0 Å < r < 25 Å and 0 < φ < π, resulting in a bin width of 0.25 Å for r and 1.8° for φ.

The statistical error due to incomplete sampling in calculating $\omega(r,\varphi)$ with a finite value of N_{MD} in eq 5 was estimated in the following manner. The total simulation run was divided into M segments of equal length, and for each of these segments the PMF was independently calculated. The average standard deviation from the PMF for $M = 1$ is an estimate of the desired statistical error and is evaluated as follows:

$$\sigma_M = \left\langle \left\{ \frac{1}{M} \sum_{i=1}^{M} [\omega_i(r,\varphi) - \omega_{tot}(r,\varphi)]^2 \right\}^{1/2} \right\rangle_{r,\varphi} \quad (6)$$

where $\omega_i(r,\varphi)$ is the PMF, as defined in eq 4, calculated from simulation data from the ith segment and $\omega_{tot}(r,\varphi)$ is calculated from the whole simulation. The average in the angular brackets spans over the whole $\{r, \varphi\}$ space.

3. Results

3.1. Experimental. To determine the fluorescence quenching efficiency and aspects of the quenching mechanism of the dyes by Trp, steady-state and time-resolved fluorescence intensities of R6G and MR121 were measured as a function of the Trp concentration in phosphate-buffered aqueous solution. Plots of the inverse-normalized steady-state fluorescence intensities and inverse-normalized fluorescence lifetimes of the dyes vs the Trp concentration allow thermodynamic and kinetic quenching data to be determined via Stern−Volmer analysis (Figure 4). The corresponding plots for the dye/quencher pair R6G/Trp are shown in Figure 4a along with those for MR121/Trp (Figure 4b: data taken from ref 6) for comparison. The Stern−Volmer data from both dye/Trp systems are summarized in Table 1.

The bimolecular dynamic quenching rate, $k_{q,d}$, i.e., the rate at which fluorescence-quenched collisional encounter complexes between the dye and Trp are formed, can be extracted from the fluorescence lifetime data according to the "dynamic" Stern−Volmer equation:

$$\frac{\tau_0}{\tau} = 1 + k_{q,d}\tau_0[\mathrm{Trp}] \quad (7)$$

where τ denotes the measured fluorescence lifetime, τ_0 the lifetime of the free dye in solution, and [Trp] the Trp concentration. This diffusion-controlled process leads to a reduced fluorescence lifetime of the dye in the presence of Trp.

The fluorescence photon decay distributions (i.e., the time dependence of the fluorescence intensity) of the dyes were found to fit well a monoexponential model in the presence of Trp with a lifetime which is close to that of the free dye. This indicates that the complexes are essentially nonfluorescent, i.e., they exhibit a fluorescence lifetime shorter than the time-resolution of the instrument (~50 ps) used to measure the fluorescence decays. Table 1 shows that $k_{q,d}$ is the same for both systems to within experimental error, whereas τ_0 is significantly longer for R6G.

Complex formation between dye and Trp reduces the amount of free fluorescent dye in solution and therefore also reduces the fluorescence intensity of the measured ensemble. The static

(30) Hill, T. L. In *Statistical Mechanics, Principles and Selected Applications*; Dover Publications, Inc.: New York, 1956; pp 179−285.

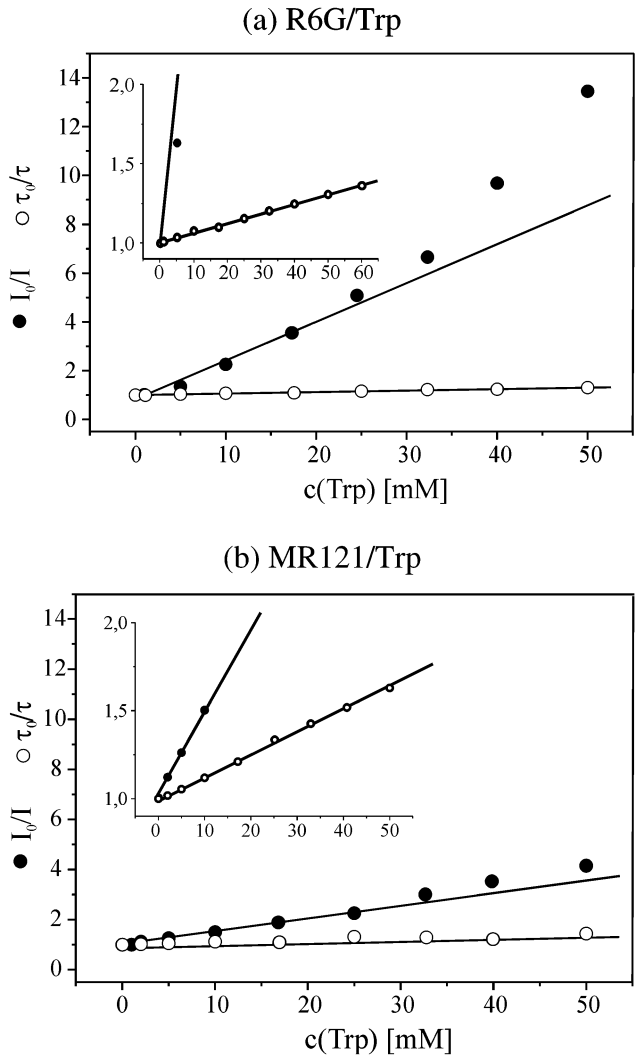

Figure 4. (a) Static (closed circles) and dynamic (open circles) bimolecular Stern−Volmer plot of R6G/Trp in phosphate-buffered saline solution, pH 7.4. Excitation wavelength: 495 nm, detection wavelength: 555 nm. (b) An equivalent plot for MR121 is shown (data taken from ref 6). Insets represent the same data as the main graphs on an expanded *y*-axis scale.

Table 1. Experimental Fluorescence Quenching Data for the Dyes MR121 and R6G with Trp in Phosphate-Buffered Saline Solution, pH 7.4[a]

	MR121	R6G
$k_{q,d}/M^{-1}\,sec^{-1}$	$(3.2 \pm 0.3) \times 10^9$	$(3.4 \pm 0.3) \times 10^9$
K_S/M^{-1}	220 ± 20	30.4 ± 3
τ_0 [ns]	1.85 ± 0.06	3.85 ± 0.12

[a] $k_{q,d}$ denotes the bimolecular dynamic quenching rate, K_S the static Stern−Volmer constant, and τ_0 the lifetime of the free dye in solution.

Stern−Volmer constant, K_S, i.e., the thermodynamic association constant for the formation of nonfluorescent ground-state complexes between the dye and Trp, can be extracted from the slope of the linear region of the concentration-dependent steady-state fluorescence intensities according to the "static" Stern−Volmer equation:

$$\frac{I_0}{I} = 1 + K_S[\mathrm{Trp}] \tag{8}$$

where I denotes the measured steady-state fluorescence intensity and I_0 denotes the fluorescence intensity of the free dye in solution. In the case of a quenching mechanism containing both static and dynamic components, the intensity plots are nonlinear as the dependence of I_0/I becomes second order in [Trp]. This is the case here for both dye/quencher pairs.

K_S is about seven times higher for MR121/Trp than for R6G/Trp. This reveals a stronger tendency of Trp to form non- or only weakly fluorescent ground-state complexes with MR121 than with R6G.

The time-resolved fluorescence quenching experiments are consistent with a model in which the underlying quenching mechanism involves dye/quencher complex formation. This conclusion is supported by the observation that for both systems the static Stern−Volmer constant, K_S, strongly decreases upon addition of detergent or organic solvents such as ethanol (data not shown). This suggests that hydrophobic interactions between MR121 or R6G and Trp may play an important role in the formation of the nonfluorescent complexes. In this case, the mechanism would involve a PET reaction between the Trp and the dye in stacked interaction geometries, similar to that observed for the dye/quencher pair riboflavin/Trp in the riboflavin-binding protein.[3]

3.2. MD Simulation Results. To obtain an atomic-detail description of the geometries involving fluorescence quenching of the organic dyes by Trp, MD simulations were performed on the systems MR121/Trp and R6G/Trp in aqueous solution.

$\Phi_{f,rel}$ ($= I/I_0$) is the relative fluorescence quantum yield. The values of $\Phi_{f,rel}$ obtained at Trp concentrations corresponding to those used in the simulations are ~0.25 for the R6G/Trp system and ~0.10 for the MR121/Trp system, as determined from Figure 4. This corresponds to a single dye molecule being in a fluorescent state for ~25% of the observation time for R6G and ~10% for MR121. The question arises as to what geometries correspond to the nonfluorescent states for the two systems. To examine this, the one-dimensional, normalized probability distribution, $P(r)$ of the dye-quencher distance r, was calculated from the simulations. The results are shown in Figure 5. The probability distributions of the two dye/quencher systems are significantly different, with a higher relative population at $r > 5$ Å for R6G.

The solid line in Figure 5a,b is the integral of $P(r)$:

$$F(r^*) = \int_0^{r^*} P(r)\,\mathrm{d}r \tag{9}$$

$F(r^*)$ is thus the fraction of configurations observed for which $r < r^*$. Using the above-determined experimental probability values of $F = 75\%$ for R6G/Trp and $F = 90\%$ for MR121/Trp, we can calculate the corresponding distances r^* from Figure 5. These distances, shown by dotted lines in Figure 5, are $r^* = (5.5 \pm 0.4)$ Å for R6G/Trp and $r^* = (5.4 \pm 0.2)$ Å for MR121/Trp. The error in r^* was estimated in the same manner as the error σ_5 in the PMF landscape described in eq 6. These two r^* values are remarkably similar given the significantly different form of the probability distributions $P(r)$ for the two systems. Configurations occurring at distances >5.5 Å may be considered to be fluorescent. The minimum of the Lennard-Jones potential for the carbon atoms on the ring systems is at ~2.0 Å. Therefore, the values of r^* derived above indicate that quenched configurations occur for both dyes only at distances close to contact with the Trp.

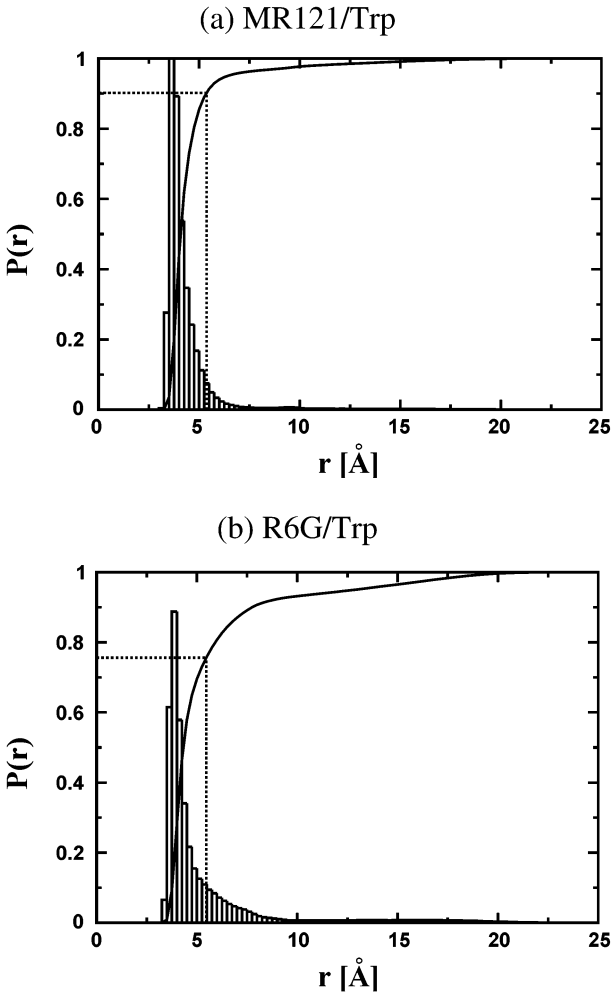

Figure 5. Normalized probability distributions $P(r)$ for MR121/Trp (a) and R6G/Trp (b). The continuous line is the integral of $P(r)$, i.e., $F(r^*)$ defined in eq 9. The dotted line indicates the value of $r^* = (5.4 \pm 0.2)$ Å for MR121/Trp and $r^* = (5.5 \pm 0.4)$ Å for R6G/Trp, corresponding to the experimental quenching efficiencies of 90 and 75%, respectively. The relative difference between the values of $F(r^*)$ for the two dyes is $\Delta F(r^*) = (15 \pm 4)\%$. The error in r^* was estimated in the same manner as the error σ_5 in the PMF landscape described in eq 6; the estimated error in $\Delta F(r^*)$ is back-propagated from the error in r^*. The trajectories were divided into five segments of equal length, and for each of them r^* was calculated. The standard deviation from the value of r^* derived from the whole simulation gives the error shown above.

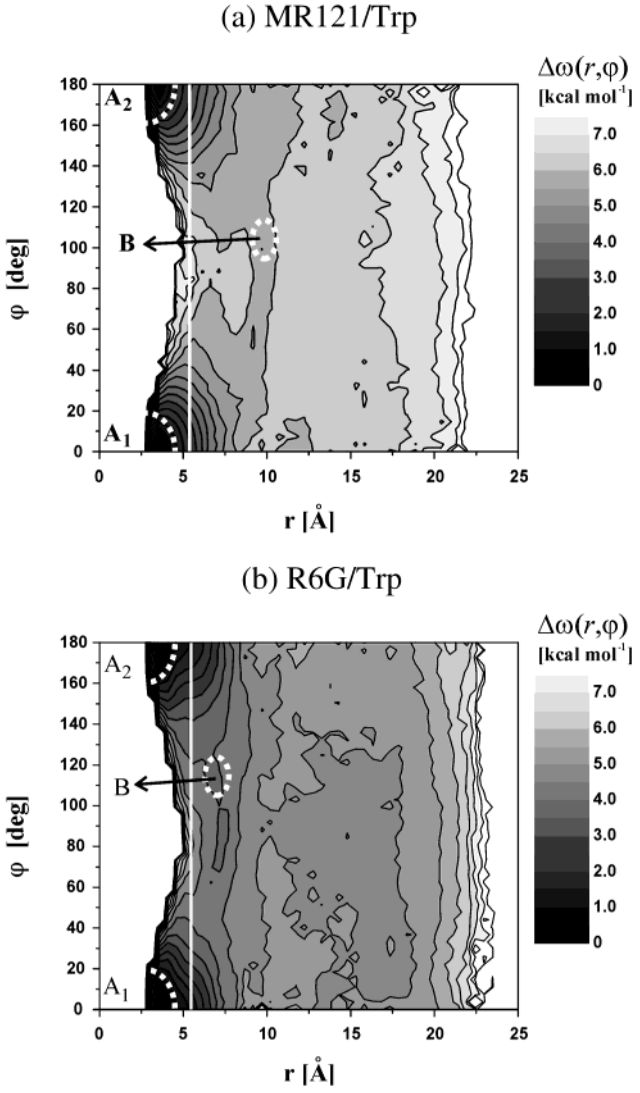

Figure 6. Two-dimensional PMF landscapes, $\Delta\omega(r,\varphi)$ derived using eq 4 for MR121/Trp (a) and R6G/Trp (b). For both, the PMF value is set to 0 kcal mol^{-1} at the global minimum. Dashed, white lines serve as a guide to the eye and mark respectively the areas A_1, A_2 (locations of the two PMF minima corresponding to close, stacking configurations of the complexes), and B (along the connection pathway between the minima) selected for subpopulation analysis (see Figures 7 and 8). The continuous white lines are placed at the quenching distances $r^* = 5.5$ Å for MR121/Trp and $r^* = 5.4$ Å for R6G/Trp.

To provide further details on the geometries of the complexes, two-dimensional $\{r, \varphi\}$ PMF maps calculated from the MD simulations are shown for both systems in Figure 6. Values of the statistical error σ_M, calculated using eq 6, are reported for $M = 2$ to $M = 7$ in Table 2. These values indicate a statistical error in the PMF landscape in the range 0.21−0.43 kcal mol^{-1} for R6G/Trp and 0.16−0.38 kcal mol^{-1} for MR121/Trp. These are similar to the values in the range 0.26−0.31 kcal mol^{-1} obtained in a recent MD analysis of the PMF landscape of aromatic amino acid complexes in water.[31]

Table 2. Values of σ_M, the Average Standard Deviation of the PMF for M Segments of Simulation, as Calculated from Eq 6 for Both Dye/Trp Systems

M	σ_M (MR121) [kcal mol^{-1}]	σ_M (R6G) [kcal mol^{-1}]
2	0.16	0.21
3	0.29	0.29
4	0.31	0.33
5	0.34	0.36
6	0.37	0.39
7	0.38	0.43

The continuous white line in Figure 6 is placed at the quenching distance $r = r^*$. To a first approximation the landscapes exhibit similar topologies. Both possess two pronounced minima labeled A_1 and A_2. These minima correspond to close-contact stacking of the ring systems of the dye with the tryptophan, well within the quenching distance. A clearly visible "low-energy" pathway connects the two minima and extends beyond the quenching distance. The PMF barrier along the pathway for the MR121/Trp system is ∼5 kcal mol^{-1}, about 1 kcal mol^{-1} higher than that of the R6G/Trp system. Both minima A_1 and A_2 are ∼1 kcal mol^{-1} shallower for R6G/Trp than for MR121/Trp. In contrast to the R6G/Trp landscape, the

(31) Chelli, R.; Gervasio, F. L.; Procacci, P.; Schettino, V. *J. Am. Chem. Soc.* **2002**, *124*, 6133−6143.

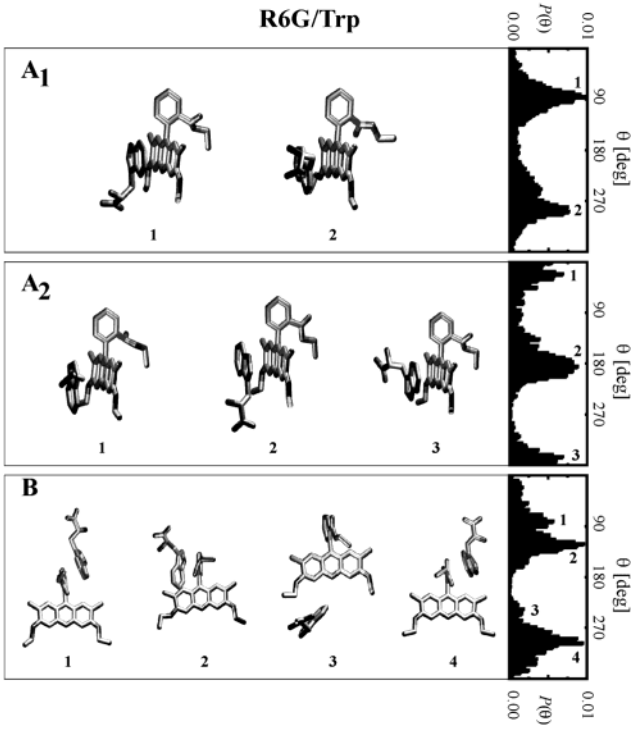

Figure 7. Average structures of the most populated subpopulations of the R6G/Trp complex occurring during the simulation runs within the areas defined in Figure 4 and marked A_1 (top panel), A_2 (middle panel), and B (bottom panel). Corresponding probability distributions of the angle θ are on the right of each panel.

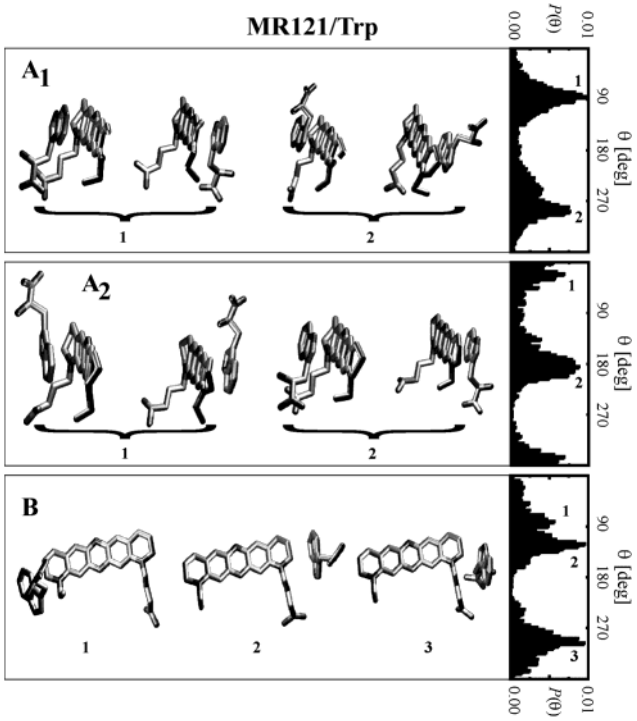

Figure 8. Average structures of the most populated subpopulations of the MR121/Trp complex occurring during the simulation runs within the areas defined in Figure 6: A_1 (top panel), A_2 (middle panel), and B (bottom panel). Corresponding probability distributions of the angle θ are on the right of each panel.

PMF of the MR121/Trp complex is almost symmetrical around $\varphi = 90°$; this reflects the fact that MR121 has planar symmetry, whereas in R6G this symmetry is broken due to the presence of the ester side chain. In both systems, beyond a separation distance of ~10 Å the PMF exhibits no significant dependence on φ.

We now examine more closely subpopulations of the stacked configurations A_1 and A_2 as well as the configurations falling in the areas along the low-energy configurational pathway between the minima (the area marked as B in Figure 6a,b). We define θ as the angle between a fixed vector on the dye plane and a fixed vector on the Trp plane (see Figure 3b). Subpopulations can be then classified according to the distribution of θ within each region A_1, A_2, and B. The Cartesian coordinates of the most frequently occurring configurations (i.e., those configurations falling within the peaks of the θ distribution) were averaged to obtain a representative structure of each subpopulation; these are shown in Figures 7 and 8.

For the R6G/Trp system, stacking of the Trp occurs only on one side of the dye plane, whereas stacking on the other side is hindered by the presence of the R6G ester group. In contrast, due to the symmetry of the MR121 dye, in the MR121/Trp system the Trp interacts with both sides of the MR121 plane. The resulting average structures within A_1 and A_2 for MR121 consist of two pairs of almost perfect mirror images (panels marked A_1 and A_2 in Figures 7 and 8). The fact that the free-energy minima (A_1 and A_2 in Figure 6) are shallower for R6G than for MR121 is also due to the presence of the ester group on R6G, which sterically hinders the dye/Trp interaction. This effect might conceivably be reduced in rhodamine derivatives that have smaller groups at the ester position.

The average structures of the complexes along the connection/escape pathway between minima are shown in panel B of Figures 7 and 8. The most frequently occurring configurations for the R6G case (Figure 7, panel B) are those in which the Trp interacts mainly with the phenyl ring of the rhodamine dye (pictures 1, 2, and 4 from the left). Visual inspection of the simulation trajectories showed that these configurations often lead to escape/entrance of the tryptophan to/from regions of the landscape beyond $r = 10$ Å. Interactions between the Trp and the phenyl ring of R6G, which are obviously not present in the case of MR121, are responsible for the fact that in Figure 5 $P(r)$ of R6G is higher than MR121 in the region 5−10 Å. This Trp/phenyl ring is a nonquenching interaction as is the Trp/ester group interaction mentioned in the previous paragraph. These two interactions compete with the quenching complexed geometries. For the case of MR121 (Figure 8, panel B), detailed inspection of the trajectories revealed that the Trp is most often found to slide along the MR121 plane before actually separating from the dye.

The bimolecular dynamic quenching rate, $k_{q,d}$ can be derived from the reduction in the average fluorescence lifetime, τ (eq 7), of the dye in the presence of quencher relative to the free dye. This reduction is due to dye/Trp collisional encounters that quench the dye fluorescence earlier than the decay from the excited state of the free dye. τ (or equivalently $k_{q,d}$) is a purely dynamical quantity: it represents the average duration of nonquenched states of the dye, and it is independent of K_S.

Values of τ were obtained from eq 7 using the experimental values of $k_{q,d}$ and τ_0 from Table 1 and the Trp concentrations used in the simulations, i.e., 55 mM for the MR121/Trp system and 57 mM for the R6G/Trp. The resulting values of τ are 2.20 ± 0.07 ns for R6G/Trp and 1.40 ± 0.04 ns for MR121/Trp.

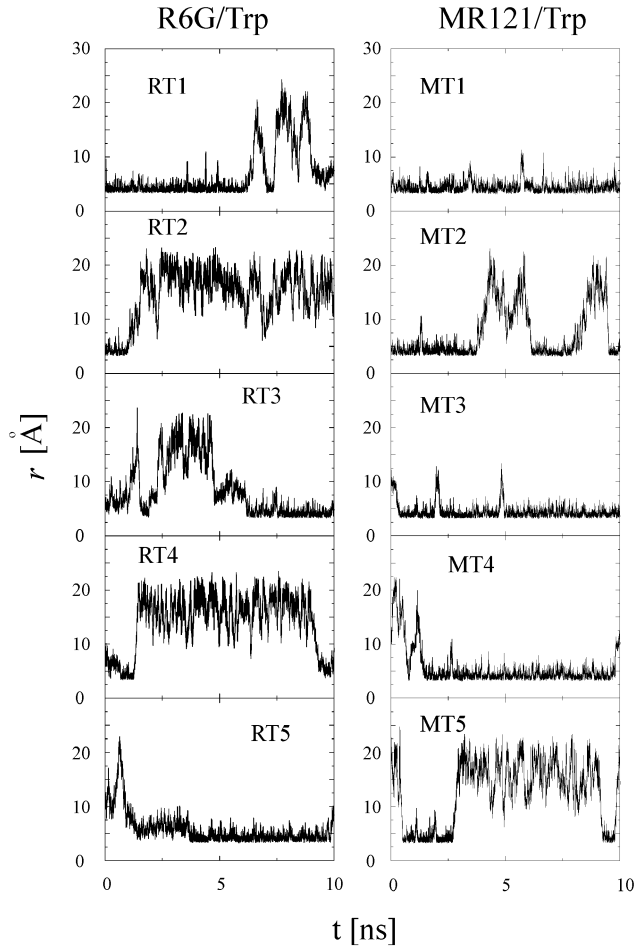

Figure 9. Time series of r during the MD runs.

In principle, τ can be estimated from MD simulation given a geometric definition of nonquenched states. The definition assumed here is as that used above: the dye is assumed to be quenched if $r < r^*$. With this definition, the duration of the ith nonquenched state occurring along the MD trajectory, $\Delta t_i = (t_{u,i} - t_{q,i})$ is simply the difference between the time $t_{u,i}$ at which the system passes from a quenched ($r < r^*$) to an unquenched ($r > r^*$) state and the time $t_{q,i}$ at which it returns to a quenched state. τ is calculated from the MD data in a similar manner as for the experiment, i.e., by fitting an exponential decay function to the probability distribution for Δt_i. To compare with the experimentally measured values of τ, transitions were excluded for which Δt_i was smaller than the time resolution of the instrument (which is ~50 ps).

The time series of r during the MD runs are shown in Figure 9 for both dye/quencher systems. The total number of transitions found in the simulations is relatively small, i.e., 30 for R6G/Trp and 21 for MR121/Trp. The resulting values for τ are 1.7 ± 0.2 ns for R6G/Trp, (cf. the experimental value of 2.20 ± 0.07 ns) and 1.5 ± 0.3 ns for MR121/Trp compared to the experimental value of 1.40 ± 0.04 ns. Given the nanosecond time scale of the fluorescence lifetimes in the present systems, longer MD simulations would be required for an accurate evaluation of this property from the simulation model. Nevertheless, the values of τ obtained from the simulation agree with the experimental values rather well (to within experimental error for MR121/Trp and almost within experimental error for R6G/Trp). That τ is of the same order as the lifetime of the free species, τ_0, confirms the small contribution of dynamical quenching relative to the contribution arising from stable, nonfluorescent complexes. The predominance of static quenching is also consistent with the fact that the time series in Figure 9 evidently exhibit confined, rather than free, diffusional characteristics.

4. Conclusions

The present work demonstrates that the combination of MD simulation with time-resolved fluorescence experiments can provide an atomic detail description of the geometry and kinetics of the quenching interaction of Trp with fluorescent dyes. The MD simulations determine molecular interaction geometries which can then be matched with results from appropriate fluorescence experiments.

In both systems studied here, the quenching mechanism is mostly static and due to formation of nonfluorescent complexes. At the Trp concentration used in the simulations and experiments, the MD-derived $P(r)$ distribution extends to higher distances for R6G than for MR121 due to the population of fluorescent interaction geometries between Trp and the R6G phenyl ring and ester group. As a consequence of this difference, about 75% of the R6G dye is quenched in comparison with 90% of the MR121, as seen experimentally. Combining these observations with the MD-derived $P(r)$ allows determination of the "quenching distance" r^*. This distance turns out to be physically reasonable and very similar (~5.5 Å) for both dye/Trp systems, corresponding to close to van der Waals contact. Finally, the lifetimes of the fluorescent states are on the nanosecond time scale and agree to within experimental error for MR121/Trp and almost within experimental error for R6G/Trp, further validating the quenching distance derived. To extend our understanding of the detailed quenching process beyond the simple "quenching distance" concept used here will require quantum chemical analysis by using, for example, the geometries derived from MD simulation as input for appropriate molecular orbital calculations.

Intramolecular dye/Trp fluoresence quenching experiments are widely applied to a variety of biomolecular systems of fundamental, medical, and technological interest. Many of the interactions involved, such as those employing peptide conjugates, involve a considerably larger number of intramolecular degrees of freedom than in the systems studied here, thus complicating the obtention of converged interaction probability distributions from computer simulation. However, it is likely that with the use of, for example, coarse-grained parallel cluster computing, useful information can also be obtained using the present approach for these systems. Thus, a basis will be provided for quantitatively interpreting fluorescence quenching data in terms of the underlying molecular interaction geometries.

Acknowledgment. The authors thank G. M. Ullmann, T. Becker, and A. Tournier for fruitful discussions, Z. Cournia for access to unpublished results, K. H. Drexhage for providing the oxazine derivative MR121, and B. Costescu for skillful technical assistance.

Supporting Information Available: MR121 force field parameters (PDF). This material is available free of charge via the Internet at http://pubs.acs.org.

JA036082J